THE MOTIONS OF A MOORED SHIP IN A HARBOR BASIN

T. Sawaragi, Dr. of Eng., Professor,Dept. of Civil Eng., Osaka Univ., Osaka, Japan.
M. Kubo, Dr. of Eng., Associate Professor, Kobe Univ. of Mercantile Marine, Kobe, Japan.

ABSTRACT

In harbors affected by ocean swells,cargo handlings are often interrupted and mooring lines are broken as a result of severe ship motions[1]. In order to decrease such accidents, the moored ship motions in a harbor basin must be studied. In this paper the ship motions in the harbor basin are investigated by using three dimensional Green's function and close agreement between theoretical and experimental results can be found. New methods to reduce moored ship motion are also proposed. The efficiency of these methods is verified theoretically and experimentally.

1. INTRODUCTION

At the initial stage of harbor planning, the hydraulic experiment with respect to stillness in a harbor is usually carried out and the degree of stillness in the harbor has been traditionally evaluated by the wave height. In the field, however, the limits of cargo handling in rough sea condition are judged by the ship movements. Therefore, lately, an analysis of moored ship motions in a harbor basin has become major interest for harbor planning.

As for the ship motions, there are short-period ones induced by wind waves and swells such as surge, sway, heave, roll, pitch and yaw, and long-period ones such as surge, sway and yaw whose natural periods are decided by the moored system. Many studies concerning long-period motions of a moored ship along the quay wall in beam sea have been done. The authors have also presented a paper about the long-period ship motions induced by the harbor oscillations in an arbitrary geometry basin[2]. Therefore, in this paper, the short-period ship motions are investigated by three dimensional method.

The three dimensional analyses are divided into two methods, one is the singularity distribution method[3] and the other is the joining method of divided region[4]. The latter method is used in this paper in order to analyze the ship motions along a straight quay wall and in a slip and these results are verified by the experiments.

On the other hand, Joglekar and Kulkani[5] have proposed the mooring system with the dash-pots in order to reduce the long-period ship motion in bore tide. However, the effects of these dash-pots on the short-period ship motions was not clarified yet. In this paper, the new mooring system with dash-pots is also analyzed theoretically and experimentally.

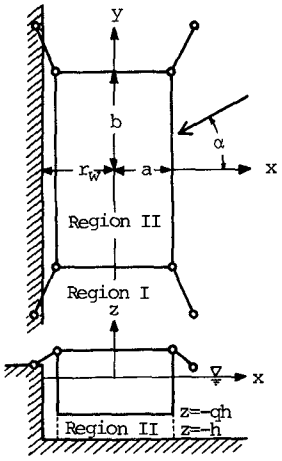

Fig.1 Definition of the coordinate system

2. THEORY OF SHIP MOTIONS

2.1 Motions of Moored Ship Along the Straight Quay Wall.

The authors will try to develop the joining method of divided region into that which can be applied to the ship motions along a straight quay wall. Since very large memory size and a great deal of cost are required in three dimensional analysis, the method of images are applied to decrease memory and cost.

Fig. 1 shows the moored ship and the coordinate system. The amplitudes of ship motions and waves are supposed to be small, and fluid around the ship is assumed to be ideal and irrotational. The coordinates of the center of gravity of the moored ship are given by $(0,0,\bar{Z}_0)$ in still water and by (X_0, Y_0, Z_0) in waves. δ_1, δ_2 and δ_3 show the rotation of the center of gravity of the moored ship around X, Y and Z axis, respectively. Then, the ship motions are expressed by:

$$X_0=\xi^* e^{-i\sigma t} \text{ (sway)}, \quad Y_0=\eta^* e^{-i\sigma t} \text{ (surge)}, \quad Z_0-\bar{Z}_0=\zeta^* e^{-i\sigma t} \text{ (heave)}$$
$$\delta_1=\omega_1^* e^{-i\sigma t} \text{ (pitch)}, \quad \delta_2=\omega_2^* e^{-i\sigma t} \text{ (roll)}, \quad \delta_3=\omega_3^* e^{-i\sigma t} \text{ (yaw)} \tag{1}$$

where ξ^*, η^*, ζ^*, ω_1^*, ω_2^* and ω_3^* are the amplitudes of ship motions, $i=\sqrt{-1}$, $\sigma=2\pi/T$, T is the wave period and t is the elapsed time. The water region is divided into two parts as shown in Fig. 1. The velocity potential in region I is given by:

$$\phi_I^w = \frac{g\zeta_0}{\sigma}[\{f_0(x,y)+f_1(x,y)\}\frac{\cosh k(h+z)}{\cosh kh} + \sum_{n=1}^{\infty} f_2^{(n)}(x,y)\frac{\cos k_n(h+z)}{\cos k_n h}] \tag{2}$$

where g is the gravitational acceleration, ζ_0 is the amplitude of incident waves, h is the water depth and the superscript w means the velocity potential along the quay wall. k and kn satisfy the following equation:

$$\sigma^2 h/g = kh \tanh kh = -k_n h \tan k_n h, \quad (n=1,2,\ldots) \tag{3}$$

The wave function f_0 corresponding to the incident and the reflected waves is given by:

$$f_0(x,y) = -i \exp\{-ik(x\cos\alpha + y\sin\alpha)\} - i\exp[-ik\{(-2\gamma_w - x)\cdot \cos\alpha + y\sin\alpha\}] \tag{4}$$

where γ_w is the distance between the quay wall and the center line of the ship, α is the angle of wave incidence. The functions $f_1(x, y)$ and $f_2^{(n)}(x, y)$ are the terms corresponding to the evanescent modes and they are expressed as Eq.(5) by using the Green's formula:

$$f_1(x,y) = -\frac{1}{2}\sum_{j=1}^{q}\{\bar{A}_{xj} f_1(j) - A_{xj}\bar{f}_1(j)\}$$

$$f_2^{(m)}(x,y) = -\frac{1}{2}\sum_{j=1}^{N}\{\bar{B}_{xj}f_2^{(m)}(j)-B_{xj}\bar{f}_2^{(m)}(j)\} \tag{5}$$

where over bars indicates the normal derivative to the boundary, namely, $\bar{f}_1(j)=\partial f_1(j)/k\partial\nu$, $\bar{f}_2^{(m)}(j)=\partial f_2^{(m)}(j)/k\partial\nu$, N is the number of segments of the boundary of ship and A_{xj}, $\bar{A}_{xj}$, B_{xj} and $\bar{B}_{xj}$ are given by:

$$A_{xj}=-\frac{i}{2}\int_{\Delta s_j}\{H_0^{(1)}(k\gamma_S)+H_0^{(1)}(k\gamma_I)\}k\,ds,\quad \bar{A}_{xj}=-\frac{i}{2}\int_{\Delta s_j}\frac{\partial}{\partial\nu}\{H_0^{(1)}(k\gamma_S)+H_0^{(1)}(k\gamma_I)\}ds,$$

$$B_{xj}=-\frac{1}{\pi}\int_{\Delta s_j}\{K_0(k_n\gamma_S)+K_0(k_n\gamma_I)\}k\,ds,\quad \bar{B}_{xj}=-\frac{1}{\pi}\int_{\Delta s_j}\frac{\partial}{\partial\nu}\{K_0(k_n\gamma_S)+K_0(k_n\gamma_I)\}ds,$$

$$\gamma_S=\sqrt{(x-\xi_j)^2+(y-\eta_j)^2},\quad \gamma_I=\sqrt{(2\gamma+x+\xi_j)^2+(y-\eta_j)^2} \tag{6}$$

where the coordinates (ξ, η) correspond to the boundary of ship, j is the number of segments of boundary of ship and the coordinates (x, y) express the internal point.

On the other hand, the velocity potential in region II is given by:

$$\left.\begin{aligned}\phi_{II}^{W}=&\frac{g\zeta_0}{\sigma}\Big[\psi_0(x,y)+\sum_{s=1}^{\infty}\psi_s(x.y)\cos\bar{s}\,(z+\bar{q}h)\\&+i\,\frac{1}{2\bar{q}}\,\frac{\sigma^2h}{g}\Big\{\Big(-\frac{\zeta^*}{\zeta_0}-\frac{\omega_1^*y}{\zeta_0}+\frac{\omega_2^*x}{\zeta_0}\Big)\Big((1+\frac{z}{h})^2-\frac{\bar{q}^2}{3}\Big)\\&+\frac{1}{4}\Big(\frac{2\zeta^*}{\zeta_0}+\frac{\omega_1^*y}{\zeta_0}-\frac{\omega_2^*x}{\zeta_0}\Big)\Big(\frac{x^2+y^2}{h^2}\Big)\Big\}\Big],\end{aligned}\right\} \tag{7}$$

where $\bar{s}=s\pi/\bar{q}h$, $\bar{q}=1-q$ and qh is the draft of the ship. When Ps are the wave forces, Ts are the moments of wave forces, Fs are the mooring forces and Ms are the moments of the mooring forces, the equations of motions of moored ship are given by:

$$\left.\begin{aligned}M\frac{d^2X_0}{dt^2}&=Px+Fx,\quad M\frac{d^2Y_0}{dt^2}=Py+Fy,\quad M\frac{d^2Z_0}{dt^2}=Pz+Fz,\\I_x\frac{d^2\delta_1}{dt^2}&=Tx+Mx,\quad I_y\frac{d^2\delta_2}{dt^2}=Ty+My,\quad I_z\frac{d^2\delta_3}{dt^2}=Tz+Mz,\end{aligned}\right\} \tag{8}$$

where M and Is are the mass and moments of inertia of the ship.

The continuity conditions of fluid particle velocity and pressure at the imaginary boundary shown in Fig. 1 are given by:

$$\left.\begin{aligned}\frac{\partial\phi_I^W}{\partial x}&=-i\sigma\{\xi^*-\omega_3^*y+\omega_2^*(z-\bar{z}_0)\},\ (\xi=\pm a,\ 0>z>-qh),\\\frac{\partial\phi_I^W}{\partial y}&=-i\sigma\{\eta^*+\omega_3^*x-\omega_1^*(z-\bar{z}_0)\},\ (\eta=\pm b,\ 0>z>-qh),\\\frac{\partial\phi_I^W}{\partial\nu}&=\frac{\partial\phi_{II}^W}{\partial\nu},\ (-qh>z>-h),\quad \phi_I^W=\phi_{II}^W,\ (-qh>z>-h)\end{aligned}\right\} \tag{9}$$

where a=B/2, B the breadth of the ship, b=Ls/2, Ls the length of the ship. From Eq.(1) to Eq.(9), the amplitudes of ship motions ξ^*, η^*, ζ^*, ω_1^*, ω_2^* and ω_3^* and the unknown functions f_1, $f_2^{(m)}$, $\partial f_1/\partial\nu$, $\partial f_2^{(m)}/\partial\nu$ are obtained.

2.2 Motions of Moored Ship in a Slip

2.2.1 Wave Height Distribution in a Slip

Since the ship motions in a slip are naturally induced by waves in a slip, it becomes important to investigate the accuracy of wave height distributions in advance of the analysis of moored ship motions in the slip. Moreover, the three dimensional analysis of the ship motions especially in a slip requires very large memory size and a great deal of cost, so the method of images are also applied to decrease memory and cost.

The region around the slip is divided into two parts, as shown in Fig. 2. The velocity potential in each region is given by:

$$\left.\begin{aligned}\phi_I &= \frac{g\zeta_0}{\sigma}\{f_0(x,y) + f_1(x,y)\}\frac{\cosh k(h+z)}{\cosh kh}\\ \phi_{II} &= \frac{g\zeta_0}{\sigma} f_2(x,y)\frac{\cosh k(h+z)}{\cosh kh}\end{aligned}\right\} \quad (10)$$

when the incident waves into the slip are given by:

$$\zeta = \zeta_0 \exp\{-i(kx\cos\alpha + ky\sin\alpha + \sigma t)\} \quad (11)$$

the wave function f_0 is expressed by:

$$f_0(x,y) = -2i\cos(ky\sin\alpha)\exp(-ikx\cos\alpha) \quad (12)$$

Using the Green's formula, the wave function f_1 and f_2 are given by:

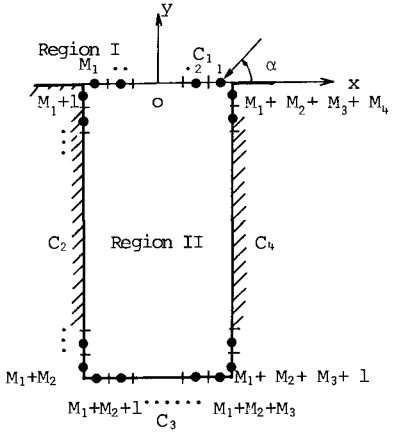

Fig.2 Division of the region around a slip and segmentation of the boundary. The angle of wave incidence is measured anti-clockwise from x-axis.

$$\left.\begin{aligned}f_1(x,y) &= -\varepsilon\sum_{j=1}^{M_1}\{\bar{A}_{xj}f_1(j) - A_{xj}\bar{f}_1(j)\}\\ f_2(x,y) &= -\varepsilon\sum_{j=1}^{N_s}\{\bar{A}_{xj}f_2(j) - A_{xj}\bar{f}_2(j)\}\end{aligned}\right\} \quad (13)$$

where M_1 is the number of segments at the entrance and Ns is the total number of segments of the slip. When (x, y) are on the boundary, ε=1/2, and when (x, y) are in the slip, ε=1.0 . It is not convenient to apply the method of images to the parallel boundaries, because the number of images amounts infinity and the times of computation becames long[6]. So the Green's functions are chosen so as to satisfy the following relations:

$$\bar{A}_{xj} = 0 \quad \text{on } C_2 \text{ , } C_3 \quad (14)$$

As the following equation is satisfied on the boundary,

$$\bar{f}_2(j) = 0 \qquad \text{on } C_2,\ C_3,\ C_4\ , \tag{15}$$

the number of segments in Eq.(13) is reduced from Ns of Lee's method to M_1+M_4. Then the Green's function A_{ij} which satisfies Eq.(14) can be obtained by the method of images as shown in Fig. 3:

$$\left.\begin{aligned}
&A_{xj}=\int_{\Delta s_j}-\frac{ik}{2}\sum_{p=1}^{4}H_0^{(1)}(k\gamma_p)\,ds,\quad \bar{A}_{xj}=\int_{\Delta s_j}\frac{ik}{2}\sum_{p=1}^{4}H_1^{(1)}(k\gamma_p)\frac{\partial\gamma_p}{\partial\nu}\,ds,\\
&\gamma_1=\sqrt{(x_j-x)^2+(y_j-y)^2}, && \frac{\partial\gamma_1}{\partial\nu}=-(y_j-y)/\gamma_1\\
&\gamma_2=\sqrt{(-x_j-2\ell_s-x)^2+(y_j-y)^2}, && \frac{\partial\gamma_2}{\partial\nu}=-(y_j-y)/\gamma_2\\
&\gamma_3=\sqrt{(-x_j-2\ell_s-x)^2+(-2ds-y_j-y)^2}, && \frac{\partial\gamma_3}{\partial\nu}=-(2ds+y_j+y)/\gamma_3\\
&\gamma_4=\sqrt{(x_j-x)^2+(-2ds-y_j-y)^2}, && \frac{\partial\gamma_4}{\partial\nu}=-(2ds+y_j+y)/\gamma_4
\end{aligned}\right\} \tag{16}$$

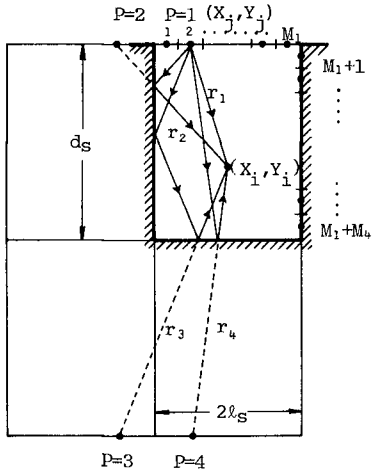

Fig.3 Reduction of number of boundary points by applying the method of images

Besides the above alternations, the computation is carried out in much the same way as the Lee's method[7]. The memory size and cost in this case is one quarter of those in the Lee's method.

Figure 4 shows the response of wave height to the wave period T. The coincidence of numerical and experimental results is fairly well. So the wave height distributions in the slip can be obtained exactly by the above method.

2.2.2 Ship Motions in a Slip

The region around the slip is divided into three parts, that is, the outer part of the slip region I, the under part of the ship region III and the rest part in the slip region II. The velocity potential in the region I is equal to Eq.(2) and is given by:

$$\phi_I^s=\phi_I^w \tag{17}$$

where the superscript s means the velocity potential in the slip. The velocity potential in the region II corresponds to the one which is lacking in $f_0(x, y)$ in Eq.(2) and is given by:

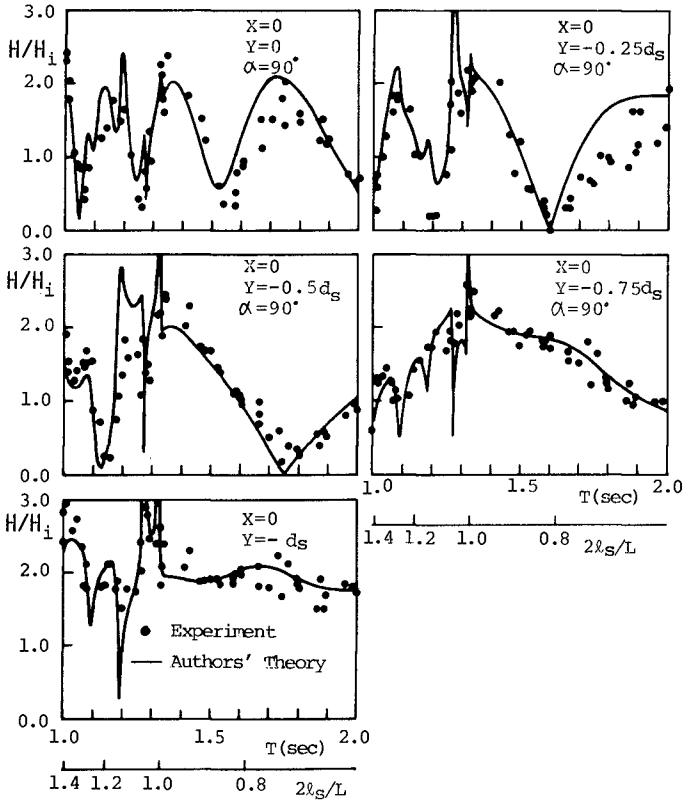

Fig.4 Amplification factor of wave height H at the typical point in the slip, where H_i is the incident wave height.

$$\phi^{s}_{II} = \frac{g\zeta_0}{\sigma}\left[\{f_2^{(0)}(x,y)\frac{\cosh k(h+z)}{\cosh kh} + \sum_{n=1}^{\infty} f_2^{(n)}(x,y)\frac{\cos k_n(h+z)}{\cos k_n h}\right] \quad (18)$$

The velocity potential in region III is the same as Eq.(7)

$$\phi^{s}_{III} = \phi^{w}_{II} \quad (19)$$

As shown in Figure 5, boundaries are chosen as follows: the entrance C_1, the quay walls surrounding the slip C_2, C_3, C_4 and the ship sides C_5. They are divided into M_1~M_5 segments.

At the entrance the following conditions must be satisfied:

$$\phi_I^S = \phi_{II}^S \ , \quad \frac{\partial \phi^S}{\partial \nu} = \frac{\partial \phi^S}{\partial \nu}, \text{on } C_1 \qquad (20)$$

Substituting Eqs.(17) and (18) into (20) and multiplying each term of above equations by cosh k(h+z) and cos kn(h+z), and integrating from z = -h to z = 0, following relations are obtained.

$$\left.\begin{aligned} f_0(i) + f_1^{(0)}(i) &= f_2^{(0)}(i), \\ f_1^{(n)}(i) &= f_2^{(n)}(i), \\ \frac{\partial (f_0(i)+f_1^{(0)}(i))}{\partial \nu} &= \frac{\partial f_2^{(0)}(i)}{\partial \nu}, \\ \frac{\partial f_1^{(n)}(i)}{\partial \nu} &= \frac{\partial f_2^{(n)}(i)}{\partial \nu}, \end{aligned}\right\} \qquad (21)$$

on C_1

where the symbol i shows the i-th position of segment instead of x,y axes. If the coastal line is straight, one of the boundary conditions is simplified as follow:

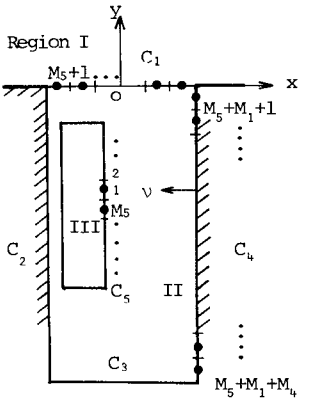

Fig.5 Definition of the coordinate system of the moored ship in the slip

$$\frac{\partial f_1^{(0)}(i)}{\partial \nu} = \frac{\partial f_2^{(0)}(i)}{\partial \nu} \ , \text{ on } C_1 \qquad (22)$$

Since the normal to the boundary is directed outward in region I, the wave function $f_1^{(0)}(i)$ is given from the Green's formula as

$$f_1^{(0)}(i) = -\frac{i}{2} \sum_{j=M_5+1}^{M_5+M_1} \{ f_1^{(0)}(j) \frac{\partial H_0^{(1)}(k\gamma)}{\partial \nu} - H_0^{(1)}(k\gamma) \frac{\partial f_1^{(0)}(j)}{\partial \nu} \} \, ds \qquad (23)$$

Substituting Eqs.(21), (22) into Eq.(23), the boundary conditions for $f_2^{(0)}(i)$ is obtained:

$$f_2^{(0)}(i) = f_0(i) + \frac{i}{2} \sum_{j=M_5+1}^{M_5+M_1} H_0^{(1)}(k\gamma) \; k\bar{f}_2^{(0)}(j) \, ds \ , \quad \text{on } C_1 \qquad (24)$$

where $\bar{f}_2^{(0)}(j) = \partial f_2^{(0)}(j)/k\partial\nu$. In the same way, the next condition can be obtained.

$$f_2^{(n)}(i) = \frac{1}{\pi} \sum_{j=M_5+1}^{M_5+M_1} K_0(k_n\gamma) \; k\bar{f}_2^{(n)}(j) \, ds \ , \text{ on } C_1 \qquad (25)$$

where $\bar{f}_2^{(n)}(j) = \partial f_2^{(n)}(j)/k\partial\nu$.

Applying the Green's formula to the boundaries C_1, C_4,C_5, the next equations can be obtained:

$$\left.\begin{aligned} f_2^{(0)}(i) &= -\sum_{j=1}^{M_5+M_1+M_4} \{ \bar{A}_{ij} \, f_2^{(0)}(j) - A_{ij} \, \bar{f}_2^{(0)}(j) \} \\ f_2^{(n)}(i) &= -\sum_{j=1}^{M_5+M_1+M_4} \{ \bar{B}_{ij}^{(n)} f_2^{(n)}(j) - B_{ij}^{(n)} \bar{f}_2^{(n)}(j) \} \\ & \qquad \text{on } C_1, C_4, C_5 \end{aligned}\right\} \qquad (26)$$

where A_{ij}, $\bar{A}_{ij}$, $B_{ij}^{(n)}$, $\bar{B}_{ij}^{(n)}$ are given as follows:

$$A_{ij} = -\frac{i}{2} \int_{\Delta s_j} \sum_{p=1}^{4} \{ H_0^{(1)}(k\gamma_p) \} k \, ds, \quad \bar{A}_{ij} = -\frac{i}{2} \int_{\Delta s_j} \sum_{p=1}^{4} \{ \frac{\partial}{\partial \nu} H_0^{(1)}(k\gamma_p) \} ds,$$

$$B_{ij}^{(n)} = -\frac{1}{\pi}\int_{\Delta s_j} \sum_{p=1}^{4} \{K_0(k_n\gamma_p)\}k\, ds, \quad \bar{B}_{ij}^{(n)} = -\frac{1}{\pi}\int_{\Delta s_j} \sum_{p=1}^{4} \{\frac{\partial}{\partial n}K_0(k_n\gamma_p)\}ds \tag{27}$$

where γ_p and $\partial\gamma_p/\partial\nu$ are equal to those given by Eq.(16).

Since the particle velocity normal to the boundary C_4 is zero, the following boundary condition is added:

$$\frac{\partial f_2^{(0)}(j)}{\partial\nu} = \frac{\partial f_2^{(n)}(j)}{\partial\nu} = 0 \text{ , on } C_4 \tag{28}$$

The above equations from (23) to (28) can be written in the matrix form:

$$\left.\begin{aligned} \mathbf{e}^{(n)} &= \mathbf{G}^{(n)} + \mathbf{H}^{(n)}\bar{\mathbf{e}}^{(n)} \\ \mathbf{f}^{(n)} &= -\bar{\mathbf{A}}^{(n)}\mathbf{f}^{(n)} + \mathbf{A}^{(n)}\bar{\mathbf{f}}^{(n)} - \bar{\mathbf{B}}^{(n)}\mathbf{e}^{(n)} + \mathbf{B}^{(n)}\bar{\mathbf{e}}^{(n)} - \bar{\mathbf{P}}^{(n)}\mathbf{X}^{(n)} \\ \mathbf{e}^{(n)} &= -\bar{\mathbf{C}}^{(n)}\mathbf{f}^{(n)} + \mathbf{C}^{(n)}\bar{\mathbf{f}}^{(n)} - \bar{\mathbf{D}}^{(n)}\mathbf{e}^{(n)} + \mathbf{D}^{(n)}\bar{\mathbf{e}}^{(n)} - \bar{\mathbf{Q}}^{(n)}\mathbf{X}^{(n)} \\ \mathbf{X}^{(n)} &= -\bar{\mathbf{R}}^{(n)}\mathbf{f}^{(n)} + \mathbf{R}^{(n)}\bar{\mathbf{f}}^{(n)} - \bar{\mathbf{S}}^{(n)}\mathbf{e}^{(n)} + \mathbf{S}^{(n)}\bar{\mathbf{e}}^{(n)} - \bar{\mathbf{T}}^{(n)}\mathbf{X}^{(n)} \end{aligned}\right\} \quad , \ n=1,2\ldots \tag{29}$$

where

$$\mathbf{G}^{(0)} = \begin{pmatrix} f_0(M_5+1) \\ f_0(M_5+2) \\ \\ f_0(M_5+M_1) \end{pmatrix}, \quad \mathbf{G}^{(n)} = \mathbf{0} \tag{30}$$

and $\mathbf{f}^{(n)}$, $\mathbf{e}^{(n)}$ and $\mathbf{X}^{(n)}$ are the vectors of the wave functions $f_2^{(n)}$ on the boundaries C_5, C_1 and C_4, respectively. $\mathbf{A}^{(n)}$, $\bar{\mathbf{A}}^{(n)}$, $\mathbf{B}^{(n)}$, $\bar{\mathbf{B}}^{(n)}$, $\mathbf{C}^{(n)}$, $\bar{\mathbf{C}}^{(n)}$, $\mathbf{D}^{(n)}$, $\bar{\mathbf{D}}^{(n)}$, $\bar{\mathbf{P}}^{(n)}$, $\bar{\mathbf{Q}}^{(n)}$, $\mathbf{R}^{(n)}$, $\bar{\mathbf{R}}^{(n)}$, $\mathbf{S}^{(n)}$, $\bar{\mathbf{S}}^{(n)}$, $\bar{\mathbf{T}}^{(n)}$ are the known matrices.

Rearranging the expression (29), the wave functions $\mathbf{f}^{(n)}$ and $\bar{\mathbf{f}}^{(n)}$ (n=1,2,...) on the ship boundary can be transformed into:

$$\bar{\mathbf{f}}^{(n)} = \bar{\mathbf{U}}^{(n)}\mathbf{f}^{(n)} + \mathbf{u}^{(n)} \ , \tag{31}$$

where $\bar{\mathbf{U}}^{(n)}$ is the known matrix and $\mathbf{u}^{(n)}$ is the known vector.

Once the relation between $f_2^{(n)}$ and $\bar{f}_2^{(n)}$ on the ship boundary is obtained, the procedure of the calculation hereafter is the same as that of ship motions along the straight quay wall.

3 EXPERIMENTAL VERIFICATION

3.1 Experimental Apparatus and Procedure

The experimental setup in cases of the quay wall and the slip are shown in Figure 6 (a) and (b), respectively. The wave basin of 30 m long, 20 m wide and 0.6 m deep was used in the experiment. A rectangular floating body of 2.4 m long, 0.455 m wide and 0.098 m deep was used as a ship model. The other dimensions of this ship model are shown in Tables 1 and 2. The ship model was moored by coiled springs whose spring constant was 67 gf/cm. The ship motions were measured by the 6-component measuring instrument.

3.2 Results and Discussion

3.2.1 Ship Motions Along the Quay Wall

The kinds of experiments of the ship motions are carried out under the following conditions. In one group, the wave period is varied and

the angle of wave incidence was kept constant and vice versa in the other group.

(a) Ship motions in beam seas

In Figure 7, the ship motions measured in experiments are compared with the theoretical results. As can be seen in the rolling motion, the calculated period of resonance is little bit smaller than that of the experiment. The reason of this difference is the effect of eddy-making which is not taken into account in this analysis. While experimental results of heaving and swaying motions seem to be predicted fairly well by this theoretical analysis.

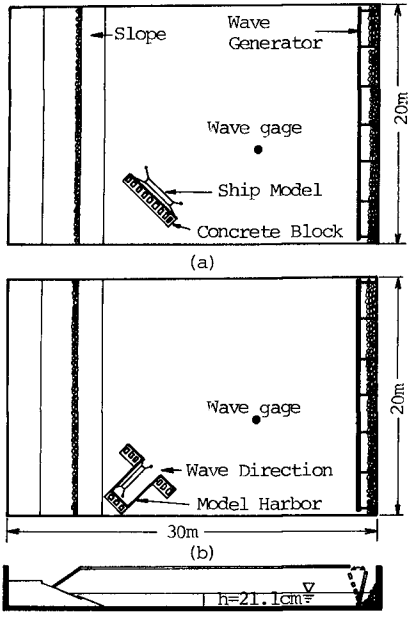

Fig.6 Arrangement of moored ship in the wave basin

If the floating body is symmetric with respect to the x-axis in beams seas, pitching, surging and yawing motions should not occur in the potential theory. Although the solid lines in Fig. 7 in these ship motions show the results considering the difference of the center of gravity from the center of figure in y-direction, there is wide division between theoretical and experimental results especially in yawing motion. The asymmetry of waves and the effect of eddy shedding may account for this discrepancy.

Table 1 Dimensions of moored ship along the quay wall

Natural period (sec)	
Sway 8.2 ,Surge 5.5 ,Heave 1.22	
Pitch 1.7 ,Roll 1.34,Yaw 3.8	
Moment of inertia	
Pitch	$486 \times 10^6 (g \cdot cm^2)$
Roll	$313 \times 10^5 (g.cm^2)$
Yaw	$497 \times 10^5 (g.cm^2)$

Table 2 Dimensions of moored ship in the slip

Natural period (sec)	
Sway 7.7 ,Surge 5.0 ,Heave 2.08	
Pitch 2.5 ,Roll 1.38,Yaw 3.89	
Moment of inertia	
Pitch	$569 \times 10^6 (g.cm^2)$
Roll	$432 \times 10^5 (g.cm^2)$
yaw	$593 \times 10^5 (g.cm^2)$

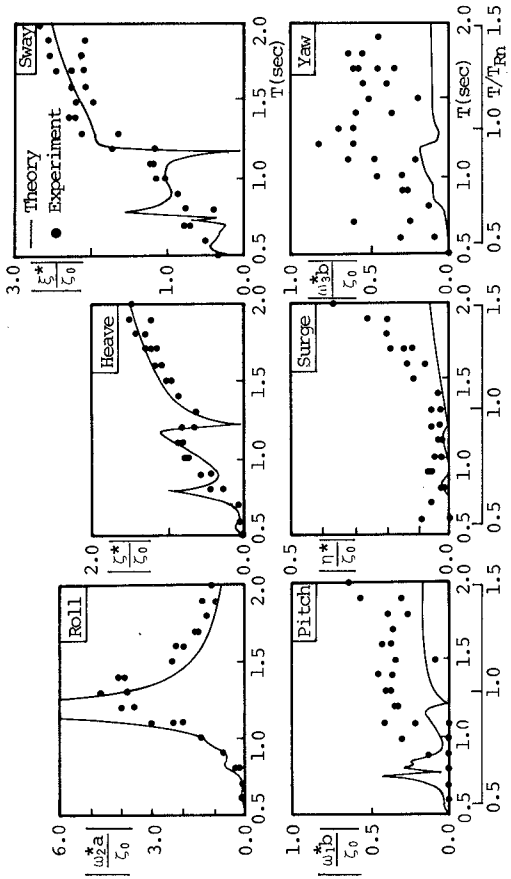

Fig.7 Motions of moored ship along the straight quay wall in beam seas

(b) Ship motions in waves of arbitrary angle of wave incidence

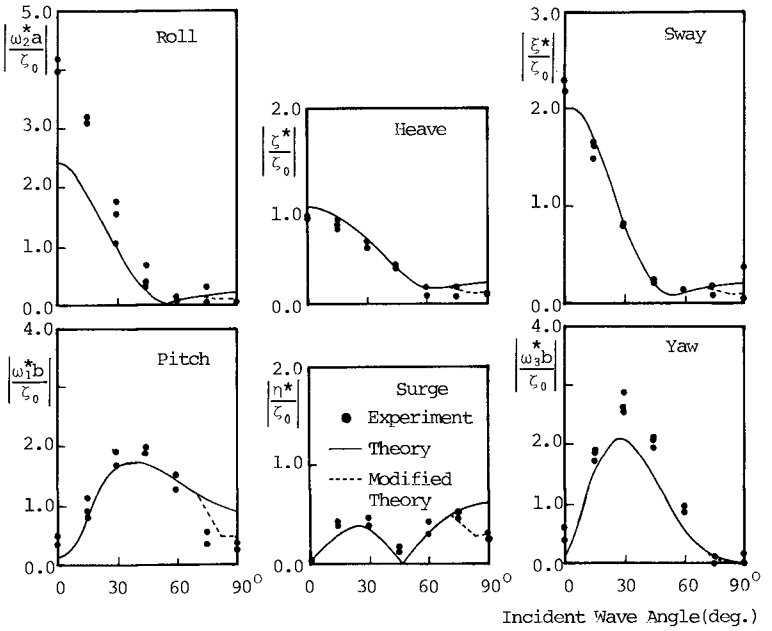

Fig.8 Relationship between ship motions and angle of wave incidence

Figure 8 shows the comparison of the experimental results with the theoretical results when the angle of wave incidence is changed from 0 to $\pi/2$. Both results show fairly good agreement. However, the theoretical results of rolling motions become smaller than the experimental ones at the small angle of wave incidence. The cause of this disagreement seems to be the difference between the numerical resonance period and the experimental resonance period as shown in Figure 7. The yawing motion in the experiment becomes larger than the theoretical one. This enlargement is thought to be caused by the eddies induced at the both ends of the ship. Finally, experimental values of almost all ship motions decrease by one-half of theoretical ones near $\alpha = 90^0$. Figure 9 schematically shows the straight quay wall of finite length and the floating body. The all reflected waves from the quay wall affect the floating body when $\alpha < \alpha_1$ but the effects of the reflected waves on the floating body become small when $\alpha_2 \geq \alpha \geq \alpha_1$, and the effects vanish entirely when $\alpha > \alpha_2$. But the reflected waves always affect the floating body in the theoretical analysis, because the quay wall is assumed to be infinity. This is the reason that experimental

results become smaller than theoretical ones near $\alpha = 90^0$. By the way, as the angle θ_{ir} shown in Fig. 9 becomes small when α approaches 90^0, the effects of the incident waves and reflected waves on the ship motions can be considered nearly equal. From the above facts, the incident wave hieght is considered one half when $\alpha > \alpha_2$ and it is considered to decrease from one to one half when $\alpha_2 \geq \alpha \geq \alpha_1$. The dotted lines show the results conducted by the above modified theory. The experimental results indicate the validity of the above way of thinking.

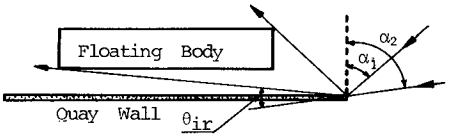

Fig.9 Reflected wave by the quay wall of finite length

3.2.2 Ship Motions in a Slip

Figure 10 shows the ship motions for three angles of wave incidence, $\alpha = 30^0$, 60^0, 90^0. It is clear from these figures that the resonance periods in a slip are different from the natural periods at the open sea. For example, the natural period in heave at the open sea is 0.8 seconds which is represented by T^o_{Hn}, but the natural period in the slip is 2.08 seconds which is expressed by T^s_{Hn} as shown in Figure 10 (b). And the natural period of the rolling motion in the slip is 1.38 seconds which is expressed by T^s_{Rn}, but the resonance periods are 1.15 seconds which are represented by T^r_{Rn} and 1.35 seconds as shown in Figure 10 (c). The resonance at T^r_{Rn} seems to be induced by the lateral oscillation which is the second mode harbor oscillations having loops at the boundaries C_2 and C_4 in Figure 5. Though T^r_{Rn} and T^s_{Rn} do not coincide each other in this experiment, the rolling motion should become large when the both resonance periods coincide.

Another important characteristics of the ship motions are the coupled resonances among mutual ship motions. Namely, as the ship is surrounded by three quay walls, the waves induced by predominant ship motions in one mode affects the other mode of ship motion. And many peaks of ship motions can be seen in Figure 10 in comparison with the ship motions along the straight quay wall or in an open sea. For example, the resonance of heaving motions at $T = T^o_{Hn}$ and T^s_{Hn} induces the new resonance in swaying and rolling motions at the same wave periods. And the resonance of rolling motions at $T = T^r_{Rn}$ and T^s_{Rn} produce the ones of swaying motions at $T = T^s_{Rn}$ and of heaving motions at $T = T^r_{Rn}$ and T^s_{Rn}. The same phenomena can be seen in the other ship motions, though they are not shown in Figure 10. By the way, since the damping forces due to eddy-shedding which will be obtained from free oscillation test are not considered in this analysis, the theoretical peaks of ship motions are fairly larger than the experimental ones. These disagreements should be improved by considering the

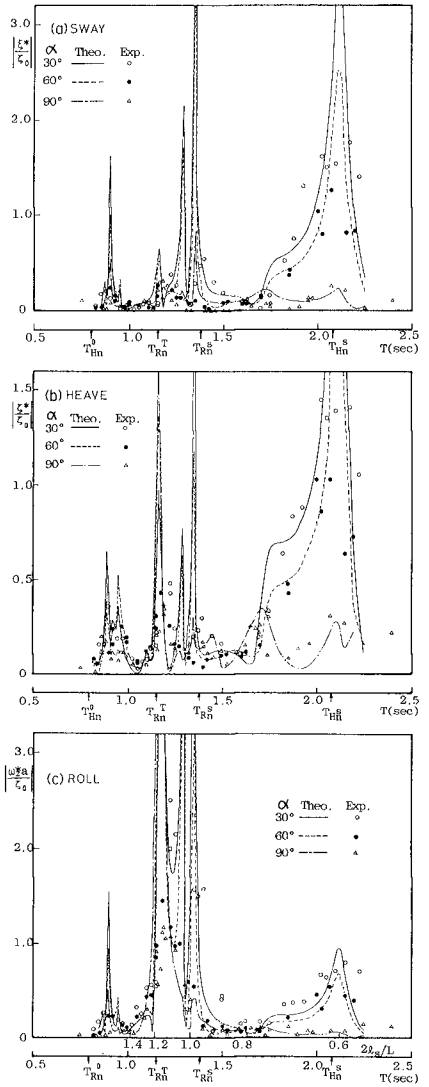

Fig.10 Ship motions in the slip

damping forces in Eq.(8). But it is clarified that the theoretical and experimental results show fairly good agreement except near the resonance periods. So it can be concluded that the short-period ship motions in the slip can be predicted by using the above potential theory.

4 MOORING SYSTEM WITH DASH-POT

The authors have already discussed the effect of the perforated quay wall[8] on the ship motions, but it was found that all ship motions along the perforated quay wall were not always smaller than those along the ordinary quay wall. So the dash-pot system is considered as the another damping system of moored ship motion[9]. In this section, the damping effect of dash-pot system on the short-period ship motion is analyzed.

4.1 Theory of Ship Motions with the Damping System

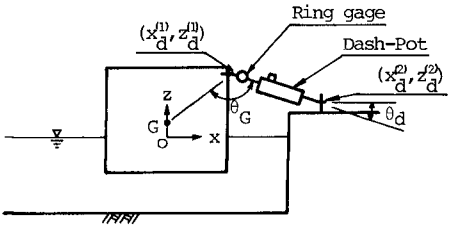

Fig.11 Arrangement of dash-pot(θ_d is measured anti-clockwise from positive x-axis)

In order to simplify the problem, it is analyzed by the two dimensional theory in the simulation. The coordinate system is shown in Figure 11. One end of the dash-pot on the ship has the coordinate $(x_d^{(1)}, z_d^{(1)})$ and the other end on the quay wall has the coordinate $(x_d^{(2)}, z_d^{(2)})$. These ends can rotate freely by universal joints. The length between both ends ℓ_d is expressed by:

$$\ell_d = \sqrt{(x_d^{(2)} - x_d^{(1)})^2 + (z_d^{(2)} - z_d^{(1)})^2} \tag{32}$$

When the ship starts to move, the end of the dash-pot on the ship moves with the ship movements, but the other end on the quay wall does not move. The change of the length of mooring line $\Delta\ell_d$ is approximated by:

$$\Delta\ell_d = \left[\frac{x_d^{(2)} - x_d^{(1)}}{\ell_d}\{\xi^* - (z_d^{(1)} - \bar{z}_0)\omega_2^*\} + \frac{z_d^{(2)} - z_d^{(1)}}{\ell_d}(\zeta^* + x_d^{(1)}\omega_2^*)\right] e^{-i\sigma t} \tag{33}$$

Since the damping force caused by dash-pot can be considered to be proportional to the velocity, the damping force F_{dp} can be given by:

$$F_{dp} = -k_d \frac{d(\Delta\ell_d)}{dt} = \hat{F}_{dp}\, e^{-i\sigma t} ,$$

$$\left.\begin{aligned}\hat{F}_{dp} = &\frac{-i\sigma k_d(x_d^{(2)} - x_d^{(1)})}{\ell_d}\{\xi^* - (z_d^{(1)} - \bar{z}_0)\omega_2^*\} \\ &\frac{-i\sigma k_d(z_d^{(2)} - z_d^{(1)})}{\ell_d}\{\zeta^* + x_d^{(1)}\omega_2^*\}\end{aligned}\right\} \quad (34)$$

where k_d is the damping coefficient. In the case of orifice with constant area, k_d is given as follow[10]:

$$k_d = \frac{8\pi\mu\ell_p A_d}{\{(a_0 + a_p)C_d\}^2}, \quad (35)$$

where μ is the coefficient of molecular viscosity, ℓ_p is the length of the orifice, A_d, a_0 and a_p are the cross-sectional areas of cylinder, orifice and piston clearance, and C_d is the coefficient of discharge. Using $\hat{F}_{dp}$, the forces $\hat{F}x$ in x-direction and $\hat{F}z$ in z-direction and the moment $\hat{M}$ are given by:

$$\left.\begin{aligned}\hat{F}_x &= -\hat{F}_{dp}\cdot\frac{x_d^{(2)} - x_d^{(1)}}{\ell_d}, \quad (36)\\ \hat{F}_z &= -\hat{F}_{dp}\cdot\frac{z_d^{(2)} - z_d^{(1)}}{\ell_d}, \quad (36)\\ \hat{M} &= -\hat{F}_x\cdot(z_d^{(1)} - \bar{z}_0) + \hat{F}_z\cdot x_d^{(1)},\end{aligned}\right\}$$

If above forces and moments caused by dash-pot are substituted into the equations of ship motions (8), the amplitudes of ship motions can be easily obtained by the same method as that of section 2.

4.2 Hydraulic Experiment

In order to verify the short-period motions of ship equipped with dash-pot, the hydraulic experiments are carried out. The arrangement of the experiment is shown in Figure 12. The sketch of the dash-pot is shown in Figure 13, and the characteristics are described in Table 3.

Both results of the ship motions with and without dash-pot are shown in Figure 14. It is found from these figures that the ship motions in every mode with the dash-pot is smaller than those without the dash-pot. Therefore, the new mooring system with dash-pot seems effective to reduce the ship motions.

Furthermore, the theoretical and the experimental results have good agreement each other. So it is clarified that the ship motions with dash-pot can be explained by the above mentioned theory. The force acting on the axis of the dash-pot is measured and is compared with the theoretical results. Both results show the same tendency, however, the theoretical one is larger than the experimental one. One reason of this difference comes from the inaccuracy of the measurement of compressive force by ring gauge. So the method of measurement should be improved hereafter.

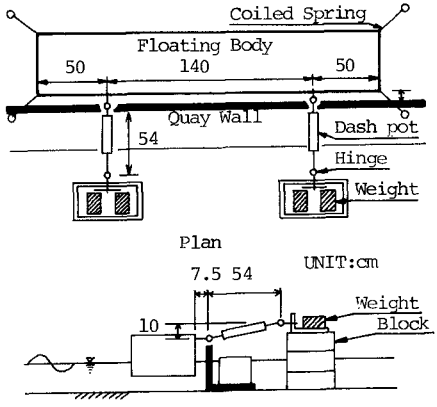

Fig.12 Experimental arrangement

Table 3 Dimensions of dash-pot

$x_d^{(1)}$	0.303m
$z_d^{(1)}$	0.197m
$x_d^{(2)}$	0.843m
$z_d^{(2)}$	0.297m
A_c	9.62cm^2
ℓ_p	10mm
a_0	14.1mm^2
a_{LR}	4.0mm^2

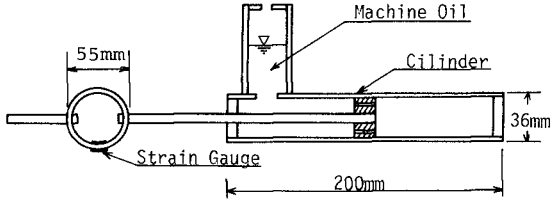

Fig.13 Dash-pot used in the experiment

4.3 Optimum Design of Dash-Pot by Numerical Simulation

Using the above mentioned theory, the optimum design of dash-pot system is investigated. Figure 15 shows the calculated ship motions and axial forces acting on the dash-pot in case of various installed angle of dash-pot θ_d. From these figures, it is found that rolling motions are significantly affected by θ_d and become smallest when $\theta_d = -57^0$, however, θ_d does not affect another nodes. On the other hand, the axial force F is the least when $\theta_d = -57^0$. As it is not favorable that the axial force which is the force acting on the bits on the ship and the quay wall is large, the angle $\theta_d = -57^0$ is the most suitable one to reduce the ship motions by dash-pot. Let θ_G be the angle as shown in Figure 11, $\theta_d = -57^0$ corresponds to $\theta_G = 90^0$. This fact shows that the dash-pot should be equipped so as to make the damping moment maximum and to suppress the rolling motion.

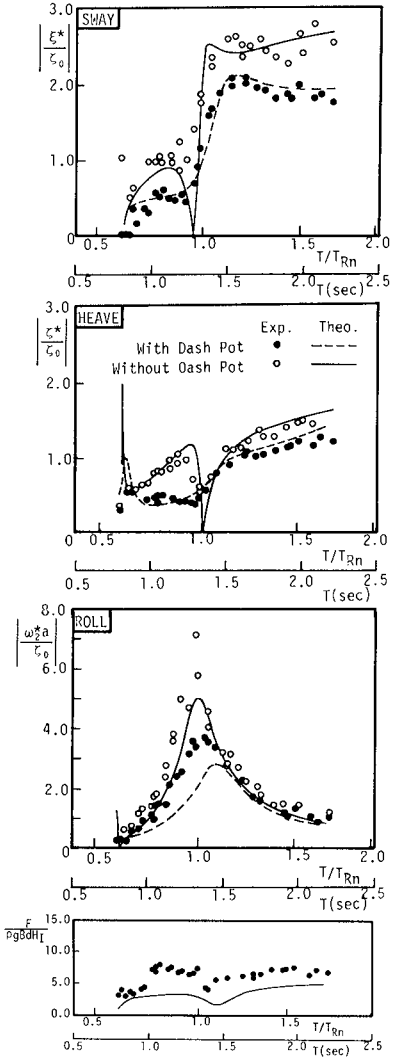

Fig.14 Comparison of ship motion with and without dash-pot, and the axial force of the dash-pot

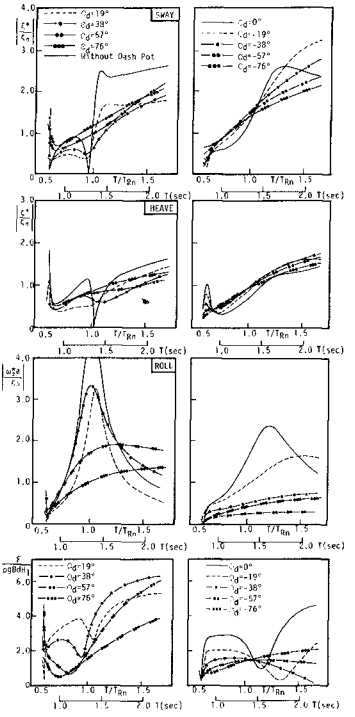

Fig.15 Ship motions and axial force of dash-pot obtained by numerical simulation

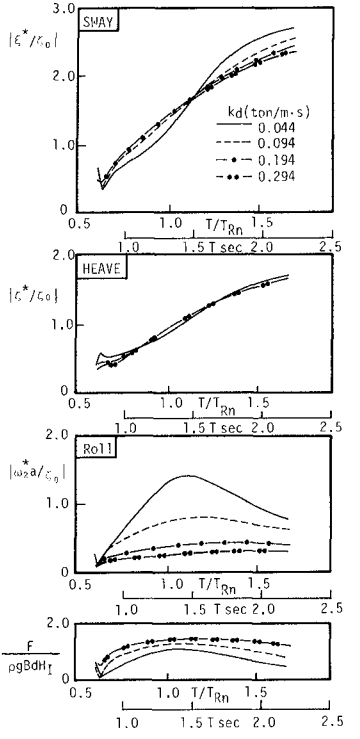

Fig.16 Relationship among ship motions, axial force and damping coefficient when $\theta_G = 90^0$

Figure 16 shows the effects of damping coefficient k_d on the ship motions and the force acting on the dash-pot when $\theta_G = 90^0$. It is noticed that the swaying and heaving motions are not heavily influenced by k_d, but the rolling motion is reduced satisfactorily with the increase of k_d.

The resonance of roll can be seen in the region when $k_d < 0.094$ ton f/(m.sec), but the resonance disappears when $k_d > 0.094$ ton f/(m.sec). The larger k_d becomes, the smaller the roll becomes. While the axial force acting on dash-pot increases. So the smallest value of k_d where the resonance of roll disappears is regarded as the optimum damping coefficient which is expressed as k_{d_0}. Though it is obtained

from the above numerical model, it can be also estimated by the following simple method.

Now, the equation of rolling motion of free oscillation is expressed by:

$$I\ddot{\delta}_2 + k_d \ell_1^2 \dot{\delta}_2 + M \cdot g \cdot GM \cdot \delta_2 = 0 \quad , \tag{38}$$

where I is the virtual moment of inertia in roll, ℓ_1 is the length between the center of gravity of the ship and the one end of the dash-pot on the ship, GM is the metercentric height. Let the natural period of roll be T_{Rn}, and define ε_R and define η_R by:

$$2\varepsilon_R = \frac{k_d \ell_1^2}{I}, \quad \eta_R^2 = \frac{M \cdot g \cdot GM}{I} \fallingdotseq \left(\frac{2\pi}{T_{Rn}} \right)^2 . \tag{39}$$

Then it can be said from the theory of mechanical vibration that the resonance of roll disappears when the following equation is satisfied [10].

$$\frac{\varepsilon_R}{\eta_R} = \frac{1}{\sqrt{2}} \tag{40}$$

The damping coefficient k_d which satisfies the above condition is also the optimum damping coefficient k_{d_0} , so by arranging the expression, k_{d_0} is obtained as follow:

$$k_{d_0} = \frac{1}{\sqrt{2}} \cdot \frac{M \cdot g \cdot GM \cdot T_{Rn}}{\pi \ell_1^2} , \tag{41}$$

Since $T_{Rn} = 0.8B/\sqrt{GM}$ [11] , Eq.(41) is rewritten by:

$$k_{d_0} = \frac{0.8}{\sqrt{2}} \cdot \frac{M \cdot g \cdot B\sqrt{GM}}{\pi \ell_1^2} \tag{42}$$

Now, for example, substituting experimental conditions M = 0.455*0.093 ton/m, GM = 0.13 m, T_{Rn} =1.3 seconds and ℓ_1 = 0.36 m into Eq.(42), k_{d_0} = 0.124 ton f/(m.sec) which is between 0.094 ton f/(m.sec) and 0.194 ton f/(m.sec) is obtained. From this, it is clear that the optimum damping coefficient can be estimated by Eqs.(41) or (42).

5 CONCLUSIONS

The motions of a moored ship in a harbor basin and the mooring system with dash-pots are investigated. The conclusions are summarized as follows:

1) The ship motions along the quay wall and in the slip can be analayzed by the three dimensional analysis.
2) Wave height distribution in the slip can be estimated by the method of images which is suitable to save cost of computation.
3) In order to reduce the short-period ship motions, a new mooring system with dash-pot is proposed. It is clarified that the system is very useful for reducing the rolling motion. Furthermore, it is clear from the numerical simulation that the angle θ_G should be

adjusted to $\pi/2$ and the optimum damping coefficient of the dash-pot is given by Eq. (42).

ACKNOWLEDGEMENT

This study is supported in part by the Research Fund of the Ministry of Education of Japan. The authors also wish to express their gratitude to Mr. S. Aoki, postgraduate student of Osaka University, who assisted us in the experiment.

REFERENCES

1) For example, Wilson,B.W.: Ship responce to range action in harbor basins, Trans. A.S.C.E.,Vol. 116,pp. 1129 - 1157, 1951.
2) Sawaragi,T. and M.Kubo: Long-period motions of a moored ship induced by harbor oscillations. Coastal Engineering in Japan, (in printing).
3) Oortmerssen,G.Van: The motions of a moored ship in waves, Publication No.510, Netherlands Ship MOdel Basin, Wageningen, The Netherlands, 1976.
4) Ijima,T.,A.Yoshida and Y.Yumura:On the motions of elliptical or rectangular floating body in waves of finite water depth, Proc. J.S.C.E.,Vol.244,pp.91 - 105, 1975 /12. (in Japanese).
5) Jogleka,D.V. and P.K.Kulkani: Mooring problems in harbors subject to seiches and tidal bores, XIXth International Navigation Congress, section II, pp. 95 - 117, 1957.
6) Sawaragi,T. and M.Kubo: Computation on wave height distribution in a slip by the method of images, The Journal of Japan Institute of Navigation, Vol. 65, pp.107 - 113, Sept.,1981. (in Japanese)
7) Lee,J.J.: Wave-induced oscillations in harbors of arbitrary geometry J.Fluid Mech. Vol. 45, pp. 375 - 394, 1971.
8) Sawaragi,T.,M.Kubo and T.Kyotani: Motions of a moored ship along the perforated quay wall, Coastal Engineering in Japan,Vol.23, pp. 277 - 286, 1980.
9) Sawaragi,T.,M.Kubo and S.Aoki: Some considerations on the method to reduce the short-period motions of moored ship by dash-pots, The Journal of Japan Institute of Navigation, Vol.66, pp. 127 - 135, 1981. (in japanese).
10) Taniguchi,O.et al.: Handbook of mechanical oscillation, Yokendo Book Company, pp. 851 - 865, 1976. (in Japanese).
11) Ohgushi,M.: Theory of ships, Vol.III, Kaibundo Book Company,Inc., pp. 25 - 30, 1961. (in Japanese).